The Influence of Needle Eccentric Motion on Hole-to-hole Injection Characteristics of a Two-layered 8-hole Diesel Injector

Tianyu Jin
School of Automotive and Traffic Engineering Jiangsu University
Zhenjiang 212013, China
Email：447438404@qq.com
Yu Sun
School of Automotive and Traffic Engineering Jiangsu University
Zhenjiang 212013, China
Email：2984313445@qq.com
Chuqiao Wang
Institute for Energy Research of Jiangsu University
Zhenjiang 212013, China
Email：cqwang@ujs.edu.cn
Adams Moro
Accra Technical University
Accra, Ghana
Email：Madams@atu.edu.gh
Xiwen Wu
Zhenjiang Campus of Army Military Transportation University
Zhenjiang 212000, China
Email：81792112@qq.com
Fuqiang Luo[1]
School of Automotive and Traffic Engineering Jiangsu University
Zhenjiang 212013, China
Email：luofq@ujs.edu.cn

Abstract

The stringent emission regulations diesel engines are required to meet has resulted in the usage of multi-hole and ultra-multi-hole injectors, nowadays. In this research study, a double layered 8-hole diesel injection nozzle was investigated both numerically and experimentally. A three-dimensional model of the nozzle which was validated with experimental results was used to analyze the injection characteristics of each hole. The validation was conducted by comparing experiment and simulation

[1] Corresponding author

injection rate results, acquired simultaneously from all the holes of the injector and the model. The fuel flow rates of the lower layered holes are higher than those of the upper layered holes. Two different needle eccentricity models were established. The first model only included the lateral displacement of the needle during needle lift. The needle reached maximum displacement at full needle lift. The second model considered the needle inelastic deformation into consideration. The needle radially displaces and glides along with the needle seat surface during needle lift. When the eccentricity reached maximum in the radial direction, the needle began to lift upwards vertically. The differences in injection characteristics under the different eccentricity models were apparent. The results indicated that the cycle injection quantity, fuel injection rate and cavitation of each hole were affected during the initial lifting stages of the needle lift. As the eccentricity of the needle increases, the injection rate uniformity from the nozzle hole deteriorates. The result showed that the upper layered holes were affected by the needle eccentricity during needle lift.

Key word: Diesel engine; Multi-hole injector; Injection rate; Needle eccentric movement

1 Introduction

The global awareness of environmental protection has resulted in the urgent need for pollutants emission reduction through efficient combustion in Internal Combustion Engine (ICE). Therefore, the continual improvement of engine combustion process through the optimization of injection processes (in terms of fuel injection rates and spray characteristics) are considered as one of the crucial methods of achieving substantial emission reduction during operation[1-3]. The fuel injection rate affects the development of fuel spray directly and the interaction with the air in the cylinder, influencing the combustion performance in the engine[4-5].

The needle is a key component in the nozzle and its reciprocating motion in the nozzle affects the injection characteristics directly[6,8]. The needle motion is not always vertical due to the gap between the needle and the needle guide. Needle guide length is limited and is not concentric with the needle valve seat. The needle experienced elastic deformation under high pressure and develops a cantilever effect when lifted[9,10]. This causes eccentricity in the radial directions, resulting in flow and injection characteristics differences among the holes, which will affect the fuel injection quality and atomization[11]. The more uneven the uniformity of the fuel distribution are, the worse the uniformity of air-fuel mixture in the combustion chamber would be, resulting in the decline of combustion quality, which ultimately affects the overall performance of the engine[12-18].

Present scholars mainly focus on the axial compression deformation of the needle and the effect of needle lift on injection characteristics[19,20]. To determine the actual motion of the needle during the opening and closing stages, researchers used various state of the art techniques to observe and measure needle lift. Moon et al.[21] used X-ray phase contrast imaging (XPCI) to analyze the transient needle movement of single-hole and multi-hole injectors. They found that the opening speed of the needle rapidly increased and then decreased during the opening period of the needle lift. When the number of holes increases, the maximum speed of opening the needle valve also decreases. Kastengren et al.[22]used X-ray phase contrast imaging technology to observe the needle movements of single-hole injector and three-hole injector. The maximum lifts of both injectors were linear to their rail pressures. To determine why the needle behaves unconditionally during the needle lift, the factors that influences the needle motion were also studied. Huang et al.[23]measured the needle motion and near-field hydrodynamic characteristics inside the nozzle. Their results show that needle lift is affected by the injection pressure during the opening stage. There is no obvious effect by extending the injection pulse width at the same injection pressure. Furthermore, the effect of needle movement on flow, injection and spray characteristics were studied extensively. Salvador et al.[24]simulated the effects of different needle lifts on the flow characteristics inside the orifice under steady state conditions. The nozzle flow coefficient reaches the maximum value at the quarter of the maximum needle lift. The higher needle lift has no great effect on the flow coefficient and fuel flow rate. Viera et al.[25]studied the relationship between the transient needle lift and the corresponding injection rate. The results show that they are not linear and are affected by the injection pressure; the needle lift speed also influences the fuel injection rate. Arienti et al.[26] simulated the spray characteristics of n-dodecane with the needle movement under adiabatic and isothermal wall conditions. As the needle gradually lifts, the gas is discharged as an incomplete jet. The calculated injection rate is smaller than those measured in the experiment due to the compressibility of the fuel.

The needle is one of the precision parts in the high-pressure common rail fuel injection system. The guide gap of the upstream needle is usually only 1-2 μm to ensure the cooperation between the needle and the needle body. X-ray phase contrast imaging and other test methods have determined that the eccentricity of the downstream needle head of different injectors ranges up to 70 μm[27]. To observe the needle displacement from different nozzles, researchers have employed various methods. Ohnishi et al.[28] drilled the head of the fuel injector. They observed the movement of the needle head in the radial direction with a high-speed camera during the fuel injection process. The results show that, for the Valve Covered Orifice (VCO) nozzle, the radial displacement of the needle radia reached 65 μm. The needle of the MicroSac (MS) nozzle has a radial displacement for 24 μm. Zhang et al.[29] used X-ray phase contrast imaging technology to observe and study the eccentric motion of injectors with different nozzle structures to analyze the influence of injection parameters, injection pressure and internal structure of the nozzle on the needle vibration. The results indicate that the axial vibration amplitude of the needle is small while the radial oscillation amplitude is from 7 μm to 14 μm, which increases with the number of injection holes. The effects of the needle displacement on fuel flow and injection characteristics were mostly investigated by means of simulation (computational methods) by various researchers. Battistoni et al.[30] used the needle eccentricity measured in the Argonne laboratory as the boundary condition to simulate the effect of the three-dimensional movement of the needle on the transient fuel flow in the porous injector. The results show that it affects the flow of fuel in the sac, resulting in the change of the parameters such as the mass flow rate at the outlet of the hole, which will affect the atomization process. Wang et al.[9] simulated the effect of needle eccentricity on the injection of the 6-hole VCO nozzle. The uniformity of the injection of each nozzle hole becomes worse as the needle valve eccentricity increases. Studies have shown that cavitation formation and spray characteristics developments are influenced to some extent by the needle eccentric movement. Powell et al.[31] used X-ray tomography and X-ray phase contrast imaging to observe the movement of the needle and the spray development at the nozzle outlet. With this technique, they observed that the fuel flow in the sac is significantly affected by the eccentric movement of the needle. Kim et al.[32] studied the effects of different needle positions on spray and internal flow characteristics in a single-hole transparent nozzle. They report that the spray cone angle and cavitation development are asymmetric as the needle position deviates. Two different directions of the two stages off-axis needle displacement were analyzed by Moro et al.[10]. Off-axis needle displacements in the immediate areas of the nozzle orifices, causes exponential increment in spray jet penetrations as compared to off-axis needle displacement around the maximum needle lift position.

Since the real nozzle hole is extremely small and the flow velocity in the nozzle hole is high, the effect of eccentric motion by the needle on the injection rate is hard to measure through experiments due to high cost and complexities[33,34]. Hence, Computational Fluid Dynamics (CFD) simulation has been used in the research of injector spray characteristics widely. A three-dimensional (3-D) model of the nozzle was used to analyze the injection characteristics of the nozzle after validating with the experimental results. The validation was conducted by comparing experiment and simulation injection rate results, acquired simultaneously from all the holes of the injector (with a customized spray momentum flux experimental test rig[35-37]) and the model. VCO nozzles exhibits higher flow sensitivities with regard to needle dynamics because of the direct relationship that exist between the needle and the orifices. The changes in flow characteristic caused by needle movement are directly propagated into the orifices. For the other nozzle types including blind hole nozzle “SAC” and mini blind hole nozzle “MicroSac”, flow characteristic changes caused by needle movement, are dampened by the sac volume to a little extent. The sac region, therefore, acts as a buffering zone between the needle and the orifices[10]. The holes on the upper and lower layers of a double-layer 8-hole sac injectors are evenly arranged circumferentially to expand the spatial distribution of the fuel and arranged as many nozzles as possible under the sac volume size. When the needle starts to move eccentrically, it will affect the fuel flow in the sac, hence influencing the fuel injection quantity of the holes. Two types of needle eccentricities were established with acceptable and reliable models. The first model considers the needle's lateral displacement during needle lift. At maximum needle lift, the needle reached its largest displacement during the eccentric movement. The second model took the needle inelastic deformation into consideration. The needle displaces radially and rise along (glides) the needle seat surface without recovering. When the maximum eccentricity in the radial direction is reached, the needle starts to rise vertically upward from the displaced position. Furthermore, the effects of different needle eccentric motions and eccentric parameters on the fuel injection rate of each hole, the cycle fuel injection quantity and the internal flow characteristics of the injection hole were analyzed in this study.

2 Mathematical model

2.1 Calculation model

Currently, homogeneous flow model, volume-of-fluid (VOF) model and two-fluid model are used to numerically study flow characteristics within nozzle hole. The two-fluid modeling approach were used to simulate the internal flow characteristics of a diesel injection nozzle in this study, since it provides the needed details with regards to flow distribution within the nozzle. This approach has been widely used in numerous research fields as it is generally considered to adequately replicate flow dynamics effectively. Using AVL Fire Eulerian-Eulerian multiphase module, the mass conservation and momentum conservation equations of the gas and the liquid phases are:

$$\frac{\partial \alpha_k \rho_k}{\partial t} + \nabla \cdot \alpha_k \rho_k v_k = \sum_{l=1, l\neq k}^{2} \Gamma_{kl} \quad (1)$$

$$\frac{\partial \alpha_k \rho_k v_k}{\partial t} + \nabla \cdot \alpha_k \rho_k v_k v_k = -\alpha_k \nabla p + \nabla \cdot \alpha_k (\tau_k + T_k^t) + \alpha_k \rho_k g$$
$$+ \sum_{l=1, l\neq k}^{2} M_{kl} + v_k \sum_{l=1, l\neq k}^{2} \Gamma_{kl} \quad (2)$$

However, the volume fraction expression (Eq. 3) has to be satisfied

$$\sum_{k=1}^{2} \alpha_k = 1 \quad (3)$$

where α_k is the volume fraction of phase *k*, ρ_k is phase k density, v_k is phase *k* velocity, Γ_{kl} is the interfacial mass exchange between phases k and l, T_k^t is phase k Reynolds stress, and M_{kl} is the momentum interfacial interaction between phases *k* and *l*. For gas phase only, *k*=1 and for liquid phase only, *k*=2.

The 4-equationsk-zeta-f turbulent model was adopted for the replication of turbulence phenomenon within the two phase flow computations[38,39].

The basic expressions of the model are the turbulent kinetic：

$$\frac{\partial \alpha_k \rho_k k_k}{\partial t} + \nabla \cdot \alpha_k \rho_k v_k k_k = \nabla \cdot \alpha_k \left(\mu_k + \frac{\mu_t^k}{\sigma_k}\right) \nabla k_k + \alpha_k P_k + \alpha_k P_{B,k} - \alpha_k \rho_k \varepsilon_k + \sum_{l=1,l\neq k}^{2} K_{kl} + k_k \sum_{l=1,l\neq k}^{2} \Gamma_{kl} \tag{4}$$

The turbulent dissipation：

$$\frac{\partial \alpha_k \rho_k \varepsilon_k}{\partial t} + \nabla \cdot \alpha_k \rho_k v_k \varepsilon_k = \nabla \cdot \alpha_k (\mu_k + \frac{\mu_t^k}{\sigma_k}) \nabla \varepsilon_k + \sum_{l=1,l\neq k}^{2} D_{kl} + \varepsilon_k \sum_{l=1,l\neq k}^{2} \Gamma_{kl} + \alpha_k C_1 P_k \frac{\varepsilon_k}{k_k} - \alpha_k C_2 \rho_k \frac{\varepsilon_k^2}{k_k} + \alpha_k C_3 \max(P_{B,k}, 0) \frac{\varepsilon_k}{k_k} - \alpha_k C_4 \rho_k \varepsilon_k \nabla \cdot v_k \tag{5}$$

The velocity scale：

$$\frac{\partial \alpha_k \rho_k \zeta_k}{\partial t} + \nabla \cdot \alpha_k \rho_k v_k \zeta_k = \nabla \cdot \alpha_k (\mu_k + \frac{\mu_t^k}{\sigma_k}) \nabla \zeta_k + \zeta_k \sum_{l=1,l\neq k}^{2} \Gamma_{kl} - \alpha_k P_k \frac{\zeta_k}{k_k} + \alpha_k f_k \tag{6}$$

The elliptical function：

$$f_k = L_k^2 \nabla^2 f_k - \frac{1}{T_k} (C_1 - 1 + C_2 \frac{P_k}{\varepsilon_k})(\zeta_k - \frac{2}{3}) \tag{7}$$

where, k_k is the turbulence kinetic energy at phase k, ε_k is the diffusivity of the turbulence kinetic energy at phase k, ζ_k is the velocity scales ratio at phase k, f_k is the elliptic function at phase k, P_k is the production term of the turbulence kinetic energy due to shear and $P_{B,k}$ is the generation component of the turbulence kinetic energy caused by buoyancy. The Prandtl number for the turbulence kinetic energy is σ_k, K_{kl} is the component of transmission between phases k and l, σ_ε is the Prandtl number for the ε equation and C_1, C_2, C_3, C_4 are constants. D_{kl} is the interfacial exchange component of the dissipation (ε) equation.

2.2 Computational meshing

The geometries of the eight holes diesel injector that is analyzed in this research is shown in

Fig. 1. The injector has a nozzle hole diameter of 0.18 mm, hole length of 0.65 mm (l_1=l_2). As seen in Fig. 1, the nozzle holes (numbered from 1 to 8 in a clockwise order) are evenly distrusted circumferentially (i.e. 45°between adjacent nozzle holes). Also, all the nozzle holes make an inclination angle of 75.5° as seen in the figure. The lower layered holes were 1, 3, 5 and 7 and the upper layered were hole 2, 4, 6 and 8. The distance between the upper layer and the lower layered was 0.12 mm.

From the nozzle geometry (shown in Fig. 1), a three dimensional (3D) model of the nozzle was developed with Pro Engineering (ProE) software as shown in Fig. 2. After a professional mesh software (Hypermesh) was used to discretize the 3D model into structured hexahedral grid shown in Fig. 3. The model was discretized into around 320,000 cells, as this quantity ensures the independence of the simulation results. As seen in Fig. 3, areas within and around the nozzle holes were meshed relatively smaller than the other areas. It is to ensure that the complex internal flow characteristic of the nozzle holes is adequately captured and analyzed. The dynamics of the needle during injection (needle movement) were simulated with moving mesh technique. With the moving mesh, transient flow characteristics with regards to needle displacement within the nozzle were obtained.

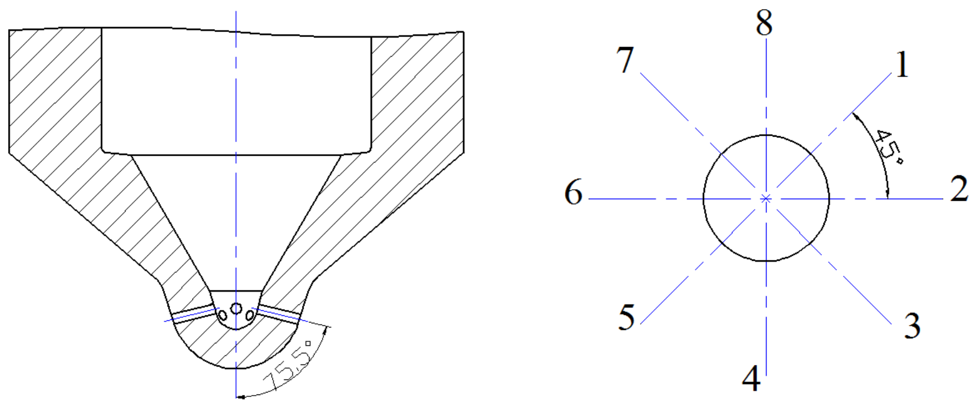

Fig. 1 Sectional views of the injection nozzle, showing the inclination angle of the nozzle hole on the left hand side

and the angle between the nozzle holes on the right hand side

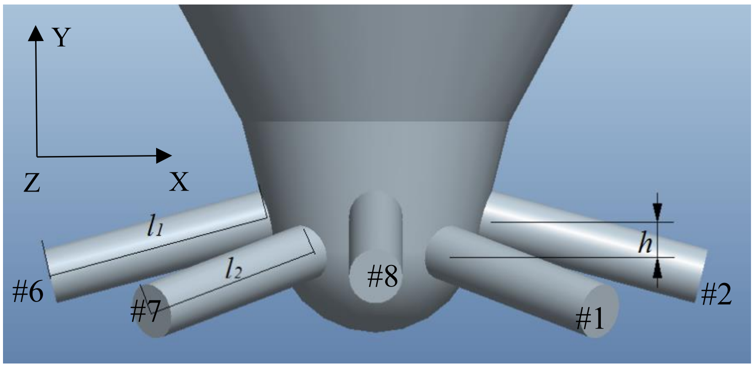

Fig.2 Sectional views of injection nozzle

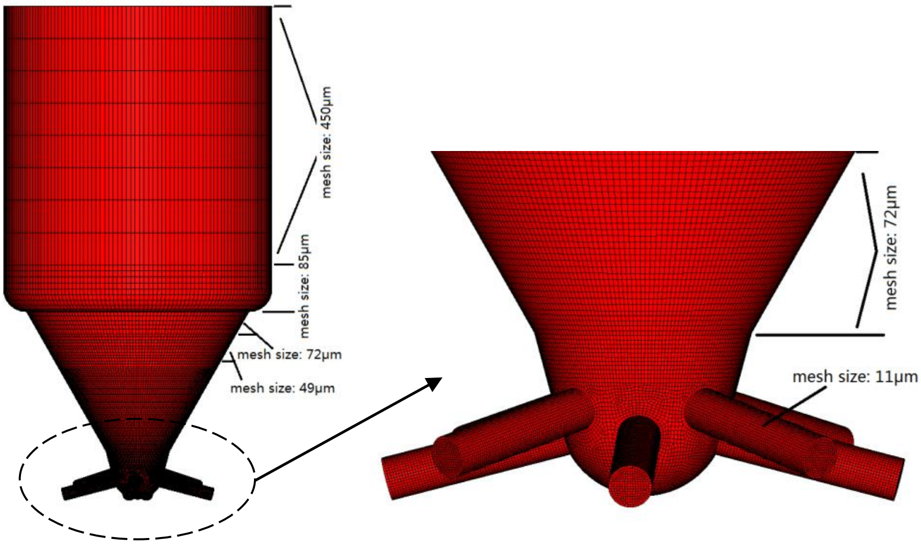

Fig. 3 The diagram of the computational grid

Since the total cell numbers of the model can influence the accuracy of the results and the computational time, it was necessary to carry out mesh sensitivity analysis firstly before conducting any investigation with the model. To ensure that the simulation results are independent of the mesh, different mesh sizes of the model were generated and then simulated. As shown in Fig. 4, the average mass flow rate obtained from the various simulations were plotted against the total mesh numbers. It can be seen from the figure that the mass flow rate begins to converge with regards to the cell numbers when cell number reached approximately 250,000. From the cell numbers of 250,000 onwards, the mass flow rate is independent of the nozzle cell number. Hence, as earlier stated, the model was discretized into around 320,000 cells totally in this investigation. The whole nozzle was modelled because it provides more flow information than a symmetric section. Even though the nozzle is a symmetric one, there will still be flow differences within the holes due to certain dynamic factors within the nozzle.

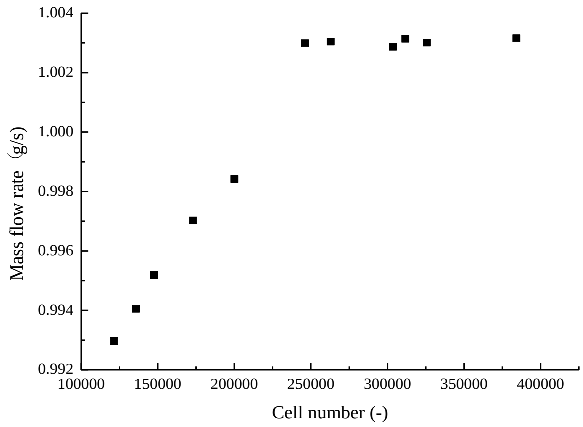

Fig. 4 Mesh sensitivity analysis

Fuel properties were set to correspond to the fuel used in experiment as well as the inlet and outlet boundary conditions.

2.3 Establishment of the needle eccentrical motion

Ideally, the nozzle needle lifted vertically upwards along the Y axis, as shown in the Fig. 5(a), which was taken as ideal model. The eccentric motion of the needle is shown in the Fig. 5(b) by the red arrow, which was taken as Model 1. The needle eccentricity is related to the nozzle structure. Although the needle movement in the entire injection process was three-dimensional, the research on the needle eccentric motion considered the lateral and the axial displacement of the needle during the eccentricity in the quest to simplify the computation. The needle reached the largest eccentricity "e" at the maximum lift. The eccentric movement in the figure is located on the X-Y plane, which passes through the centers of the nozzle hole 2 and 6. The needle radially displaces gradually towards hole 2 and away from hole 6 during the eccentric movement.

The second eccentric movement model is due to inelastic deformation of the needle (Fig. 5(c)). At the initial stages the needle displaces under high pressure towards the needle seat. This displacement results in the radial movement of the needle tip and glides along the needle seat during the lifting process (needle lift). The needle therefore experiences both radial and axial displacement during operation. The modelling of this process (needle eccentricity) was conducted in two stages. As shown in Fig. 5(c), stage 1 (shown by the red arrow 1) is the gliding stage while stage 2 (shown by the blue arrow 2) is after the gliding stage of the needle. The needle rose along with the needle seat surface during the stage 1. When the eccentricity reached to the maximum “e” in the radial direction, the needle began to lift upwards vertically until it reached the maximum lift.

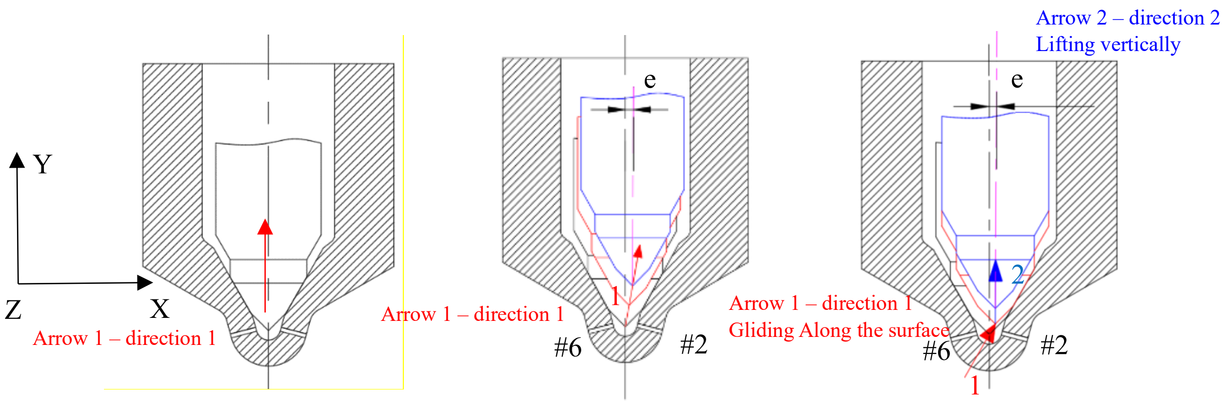

（a）Ideal model （b）Model 1 （c）Model 2

Fig. 5 Needle eccentric motion diagram

As shown in Fig. 6, two different directions of the needle eccentricities were considered. The first (0° deflection) involved the radial displacement of the needle tip towards hole 2 (i.e. away from hole 6) while the second (45° deflection) involved the radial displacement towards hole 1 (i.e. away from hole 5).

Arrow 1 -

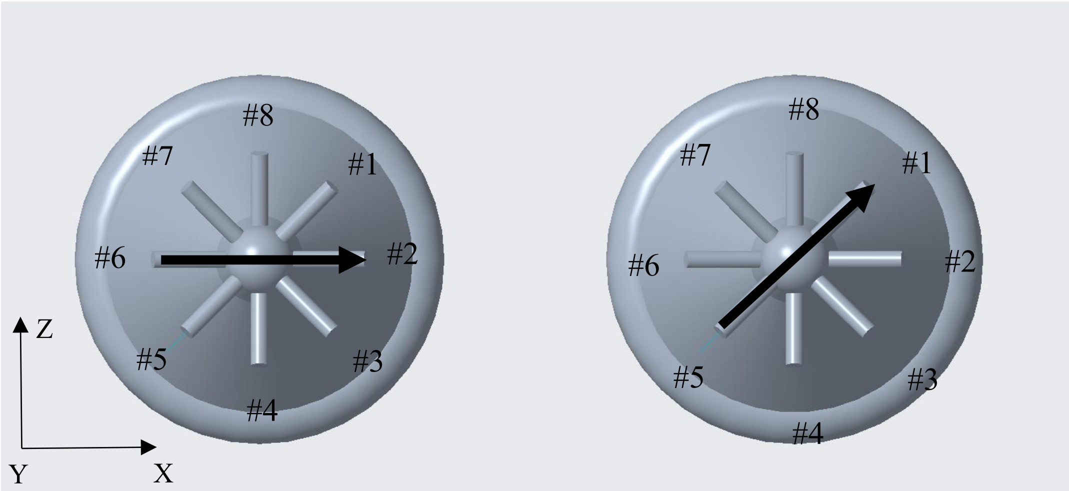

（a）0° deflection （b）45° deflection

Fig. 6 Sectional views of injection nozzle at different eccentrical direction

3 Simulation and experimental validation

3.1 Experimental equipment

The schematics of the developed spray momentum flux experimental setup used for model validation is illustrated in Fig. 7 (a). Also in Fig. 7 (b) is the pictorial view of the momentum flux experimental setup.

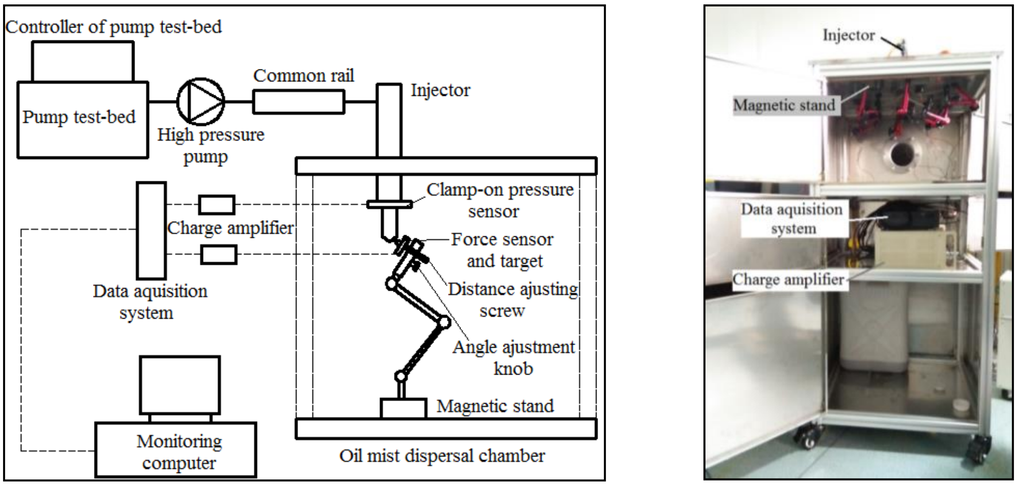

(a) (b)

Fig. 7 Diagrammatic illustrations of the experimental setup with all the sections labeled in

(a) the schematic and (b) the pictorial views respectively

It should be noted from Fig. 7 that the electronic control unit (ECU) contained in the high-pressure pump sent signals to the injector solenoid valve to be executed with regards to the operating conditions. A customized magnetic stand equipped with a distance adjusting screw and an angle adjustment knob, allowed the target-sensor assembly to be moved within the required range needed for optimum spray impact. Piezoelectric force sensors placed at required distances from the nozzle hole outlets, converted the force they experienced as a result of the spray impact on them into charge signals. The signals measured were then amplified by a charge amplifier (PPM-12KA-610) and then transmitted to a sixteen-channel data acquisition system (UA326H-16) for analysis. The data was then displayed on a computer monitor and recorded for subsequent processing[36].

3.2 Validation of the model

In this study, the validation of the model was performed at the following conditions: injection frequency of 6 Hz, injection pulse width of 2000 μs and rail pressure of 100 MPa.

The needle lift profile in Fig. 8 was prescribed and assumed based on experimental injection rate results. To simplify the model and reduce the calculation time, the lift rate at the opening and closing phase were set based on experimental results obtained in other literatures[9,10,40].

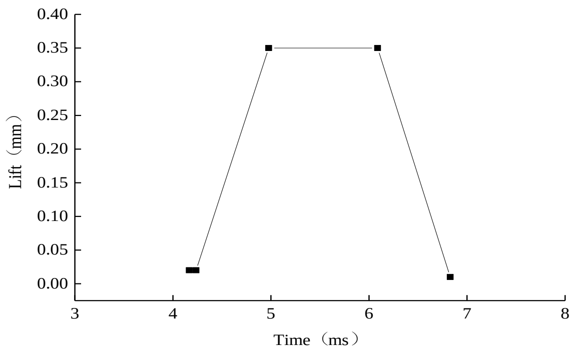

Fig. 8 The one-dimensional needle profile

The experimental injection rates were calculated by averaging 100 cycles. The cycle variation for shot-to-shot is under 1.25 % in Fig 9. Hence, ensuring the repeatability of the experiment.

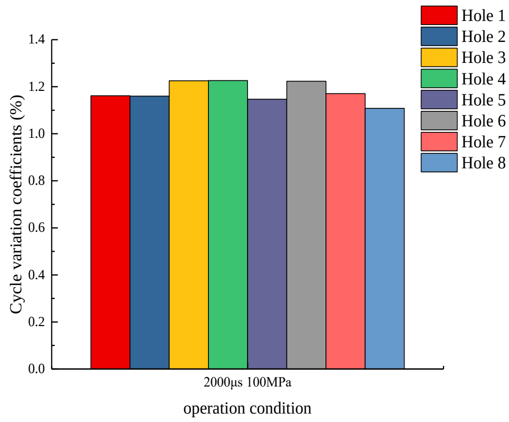

Fig. 9 Orifice-to-orifice experiment cycle variation coefficients

(Injection width pulse 2000 μs, injection pressure 100 MPa)

Fig. 10 and Tab.1 show the nozzle's hole-to-hole experimental injection rate results and the simulated injection rate results. It can be seen that the lower layered nozzle hole (1, 3, 5, 7) have higher injection rates than the upper layered nozzle holes (2, 4, 6, 8). The simulation results show that the two sets of injection rate curves are consistent with each other. They are fully in line with the expected results (theoretically). Nonetheless, it is clear from experiment results that the lower layered nozzle holes have higher injection rates than the upper layered nozzle holes

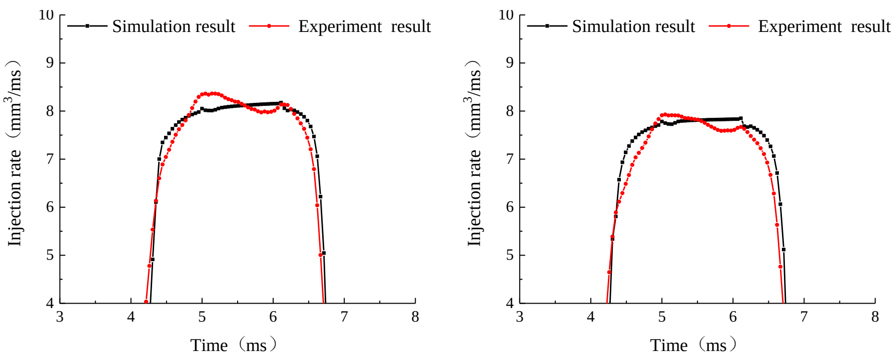

（a） Hole 1 （b）Hole 2

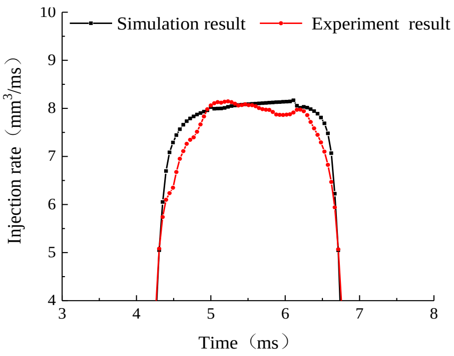

（c） Hole 3

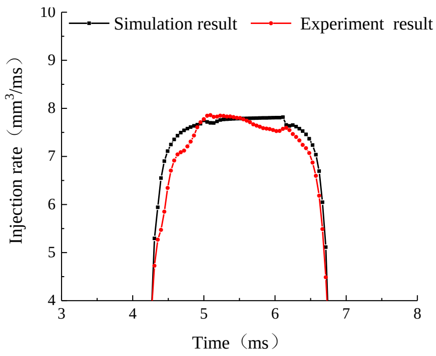

（d）Hole 4

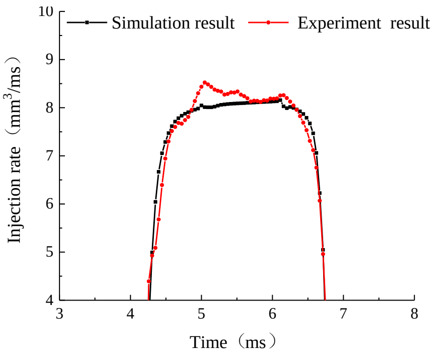

（e） Hole 5

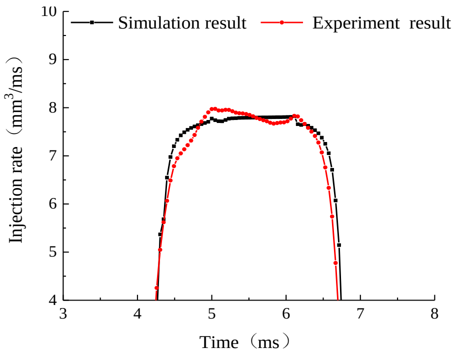

（f）Hole 6

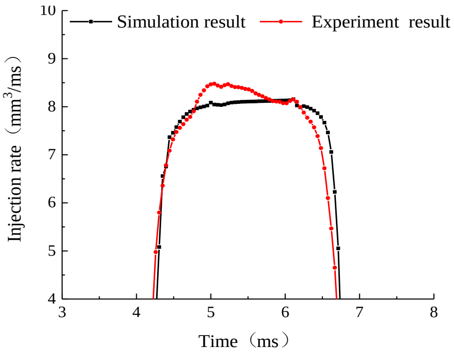

（g） Hole 7

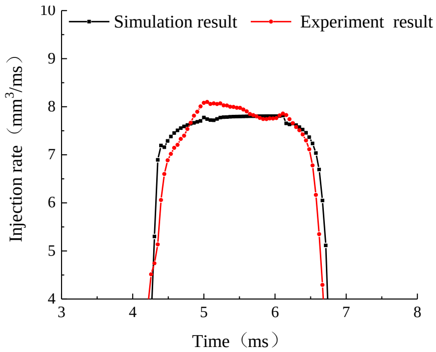

（h）Hole 8

Fig. 10 Orifice-to-orifice experiment and simulation results of injection rate comparison

(Injection width pulse 2000 μs, injection pressure 100 MPa)

Tab. 1 Orifice-to-orifice experiment and simulation results of peak rate of injection comparison

	Peak rate of injection (mm^3/ms)							
	Hole 1	Hole 2	Hole 3	Hole 4	Hole 5	Hole 6	Hole 7	Hole 8

Simulation	8.24	7.93	8.21	7.84	8.23	7.86	8.23	7.84
Experiment	8.36	7.92	8.14	7.85	8.52	7.98	8.48	8.10

Tab. 2 Orifice-to-orifice experiment and simulation results of injection quantity comparison

	Injection quantity (mm^3)							
	Hole 1	Hole 2	Hole 3	Hole 4	Hole 5	Hole 6	Hole 7	Hole 8
Simulation	19.49	18.81	19.29	18.59	19.28	18.65	19.56	18.72
Experiment	19.39	18.65	18.84	18.04	19.46	18.37	19.27	18.44

The cycle fuel injection quantity computed from simulation ($q_{simulation}$) and the cycle fuel injection quantity computed from experiment ($q_{mearsure}$)are obtained by integrating the injection rates throughout the injection duration. The relative error between the simulated and experimental result were computed with the expression:

$$\Delta_{hole} = \frac{q_{simulation} - q_{measure}}{q_{measure}} \times 100\% \tag{8}$$

From Fig. 11 and Tab.2, it can be seen that the fuel injection rates and the cycle fuel injection quantities of the lower layered nozzle holes (1,3,5,7) are 4-8 % higher than those of the upper layered nozzle holes (2,4,6,8). The relative error is under 5 %.

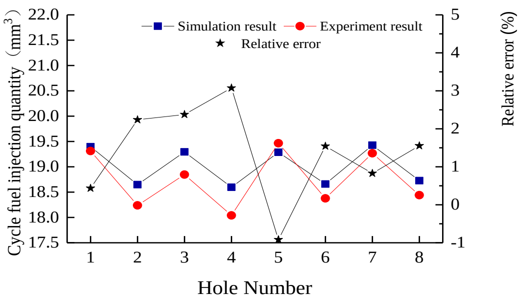

Fig. 11 Hole-to-hole experiment and simulation cycle fuel injection quantities

(Injection width pulse 2000 μs, injection pressure 100 MPa)

4 Results analysis and discussion

4.1 Effect of needle eccentricity on injection characteristics

The needle valve of high-pressure diesel injectors undergoes lateral movement and deformation, while the continuous increase in injection pressure enlarges the gap of the needle valve assembly. The previous simulation and experiment showed that the range of the needle displacement was from 0.02 mm to 0.065 mm[27,28,41]. Therefore, the radial displacement of the needle eccentricity was set to 0.02 mm 0.04 mm and 0.06 mm for the research.

The models will be classified as Ideal model for Fig. 5 (a), Model 1 for Fig. 5 (b) and Model 2 for Fig. 5 (c). The upper and lower layers are distributed equally because it is a symmetrical spray injector. The eccentric motion of the needle is radially displaced toward the injection hole 2 and away from the injection hole 6. The nozzle holes “1 and 3”, “5 and 7” and “4 and 8” are symmetric, hence only hole 1, hole 2, hole 4, hole 5 and hole 6 will be discussed next. “+” represents the rising process.

In Model 1, the injection rates of injection hole 1 and 2 begin to increase rapidly in the middle of the needle opening stage (+20 % lift~ +57 % lift) (Fig. 12 (b)). The hole 6 records the lowest injection rate. The difference among the injection rates from the same layered holes increases as the needle continuous to lift. In Model 2, the displace needle rises by gliding along surface of the needle seat in the initial stages of needle lift. It causes a narrow flow area around hole 2 and therefore restricts fuel flow through the hole. The injection rate of hole 2 has the slowest development as a result (Fig. 12(c)). The injection rate of hole 1 is not affected so much since the needle radially displaced away from it. When the needle is fully opened, the injection rates of hole 1 and 2 of the two eccentric models are higher than the injection rate of other nozzle holes in the same layer. Hole

6 has the smallest injection rate. The needle eccentricity causes asymmetric flow of fuel. Torelli[42] achieved the similar tendency.

The duration of the gliding movement by the needle on the needle guide, increases with the increase of the radial displacement of the needle. Therefore, the injection quantity of injection hole 1 and 2 of Model 2 is smaller than the injection quantities from holes 1 and 2 of Model 1. The injection quantity of hole 6 in Model 1 is the least of all the holes because the injection rate of the hole 6 is the lowest throughout the whole process. In Model 2, hole 4 has the lowest cycle injection quantity in the same layer. The needle displaced much closer to hole 4 than hole 6 during the first opening stage of the needle lift. As shown in Fig. 12 (c), the injection rate of hole 2 and hole 4 is low. The injection rate of hole 2 increases fast during the second opening stage of the needle and the injection rate of hole 4 increases slower than the rest of holes. In the fully open stage, the injection rate of hole 4 is relatively low. The closing process of the needle follows the same trend. The quantity of fuel flow in the nozzle is depicted by the density of the streamline. That is the denser the streamline the higher the quantity of fuel flow. Also, the color gives the velocity range of fuel flow from the bottom view of the nozzle. As shown in the streamline diagram in Fig. 13(c), fuel flows from hole 4 to hole 1 and also flows from hole 4 and 6 to hole 1 and hole 2 (from the streamline diagrams). Therefore, the total cycle fuel injection quantity for injection hole 4 is the lowest.

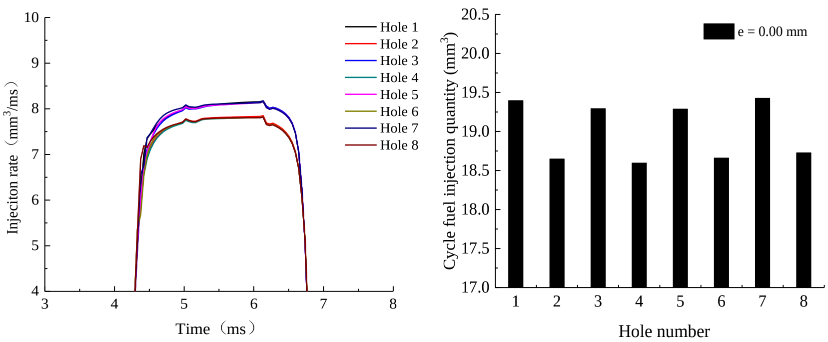

(a) Ideal model

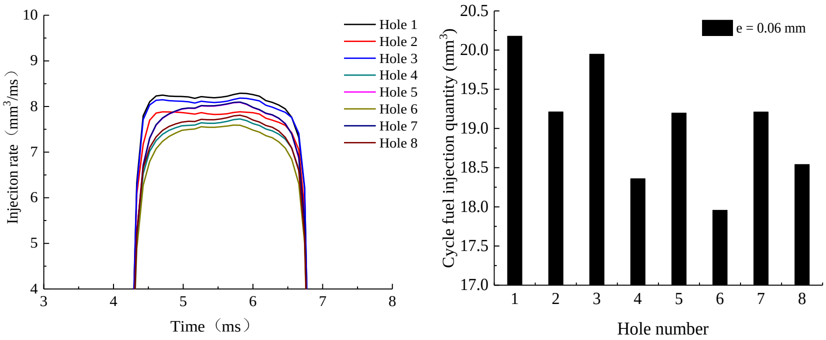

(b) Model 1

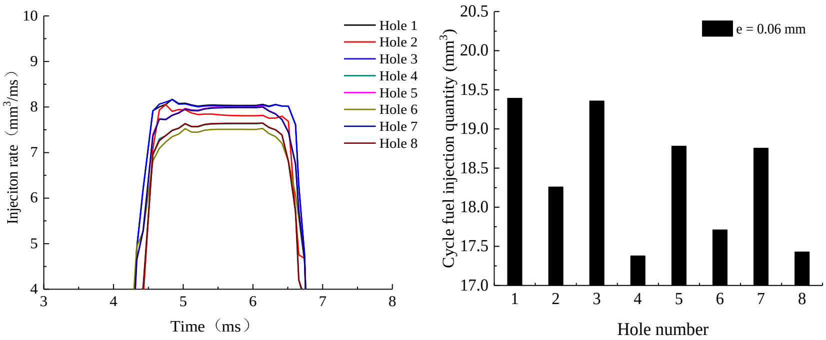

(c) Model 2

Fig. 12 Injection rate (left) and cycle injection quantity (right) of each hole with different needle valve motion models at 0.06 mm eccentricity

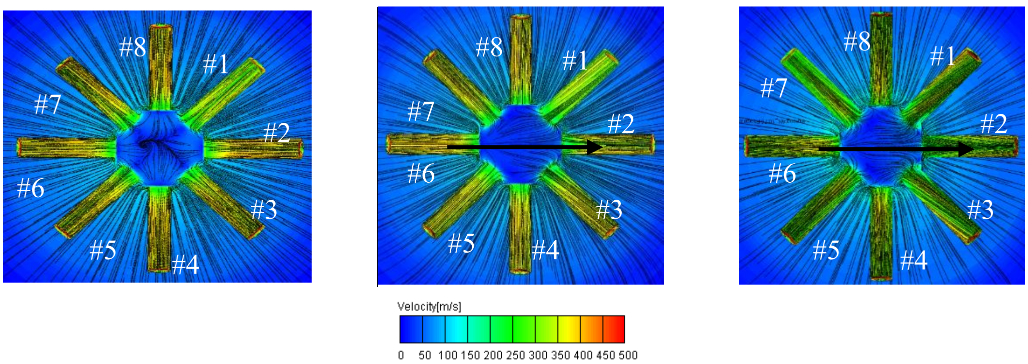

(a) Ideal model (b) Model 1 (c) Model 2

Fig. 13 Fuel streamlines of different needle motion models when the needle is fully open (bottom view)

Integrating the fuel injection rate over the entire injection duration gives the cycle fuel injection quantity of each hole. The relative average deviation is used to describe the difference in the cycle fuel injection quantity of each nozzle. The definition is:

$$\Delta_1 = \frac{q_i - q_{mean}}{q_{mean}} \times 100\% \qquad (9)$$

where q_{mean} is the average value (mm^3 / cyc) of the cycle fuel injection quantity in each hole of the injector; q_i is the cycle fuel injection quantity (mm^3 / cyc) of the hole i; Δ_1 is the relative average deviation (%).

The two needle eccentricity models have high influences on the uniformity of fuel injection from the multi hole nozzle as shown in Fig. 14. When the radial displacement of the needle reaches 0.06 mm (during eccentricity) in Model 1, the relative average deviation between the upper layered holes 2 and 6 is 6.5 % (hole 2,4,6,8 are in the same layer). The difference between the lower layered holes 1 and 5 is 5 %. The difference between hole 1 and hole 6 (from two different layers) is 11.7 %. When the radial displacement of the needle reaches 0.06 mm (during eccentricity) in Model 2, the relative average deviation between the upper layered holes 2 and 6 is 2.7 %. The difference between the lower layered holes 1 and 5 is 3.3 %. The difference between hole 1 and hole 4 (from two different layers) is 10.5 %. The degree of non-uniformity increases with increasing needle eccentricity.

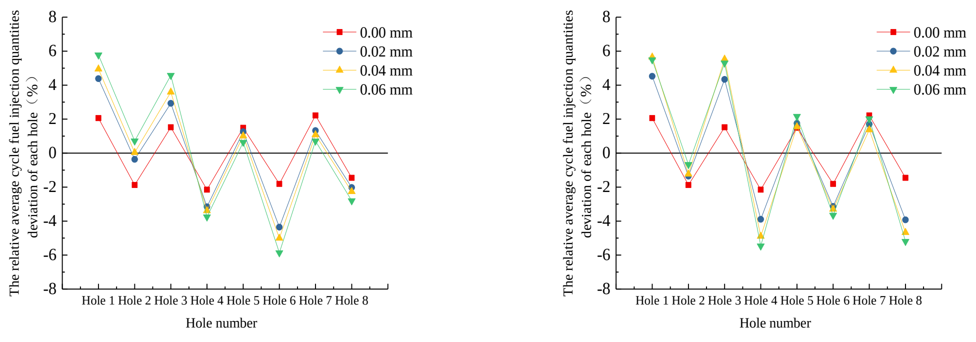

（a）Model 1 （b）Model 2

Fig. 14 Relative average deviation of hole-to-hole cycle injection quantity at different eccentricities with different needle motion models

4.2 Effect of needle eccentric parameters on fuel injection characteristics

The effects of the needle eccentricities and directions of needle displacement on injection characteristics in Model 1 were analyzed. As shown in Fig. 15, the difference in the injection rate of each hole does not change with the increase of the eccentricity in the initial stage of the needle lift. As the needle lifts, the injection rates growth rate of hole 1 and 2 increases rapidly to their maximum values as the eccentricity increases. The growth rate of hole 6 decreases with the increase of the needle eccentricity. Therefore, the fuel injection quantity of the hole 1 and hole 2 increases as the eccentricity increases. The difference in the relative average deviation of the cycle fuel injection quantity of each hole also increases as well.

When the needle displaces toward hole 1 (Fig. 15 (d)), the injection rate of nozzle hole 1 attains the highest value comparatively. When the needle is fully opened, there are no significant differences among the remaining holes on the same layer. The relative average deviation differences between the lower layered holes are not apparent (Fig. 16(b)). At eccentricity of 0.06mm, the relative average deviations of the lower layered holes 1 and 5 is 2.7 %. The difference between hole 1 and hole 4 (from two different layers) is 9 %. The lower layer holes are not sensitive to needle eccentricity because of their position with regards to the needle displacement.

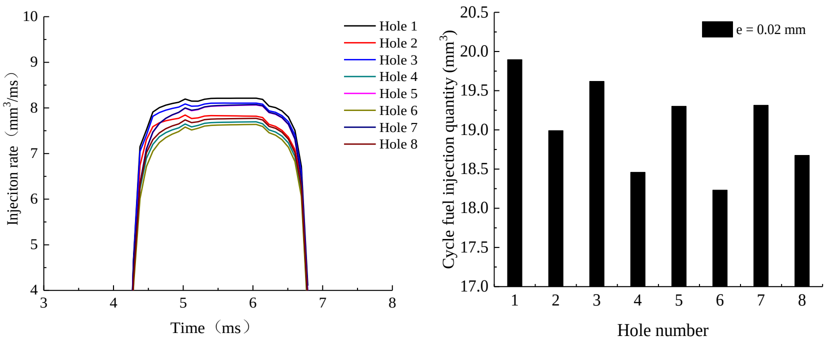

(a) e=0.02mm (0° deflection)

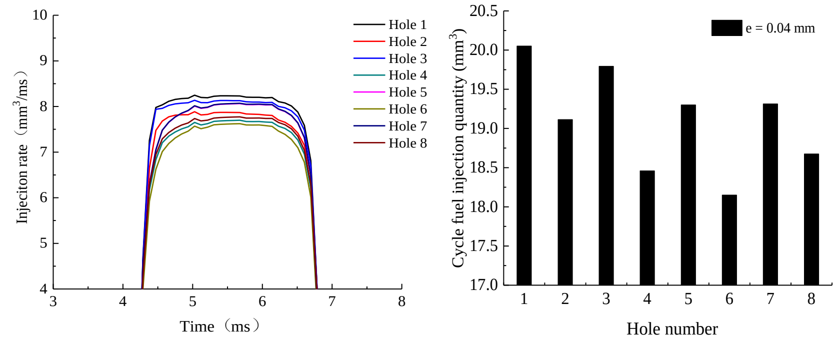

(b) e=0.04mm (0° deflection)

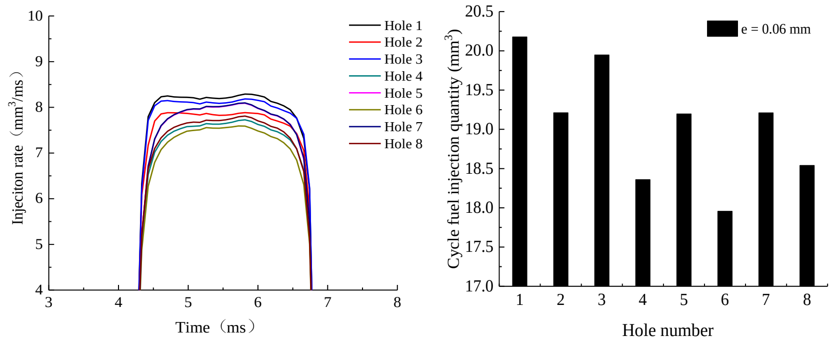

(c) e=0.06mm (0° deflection)

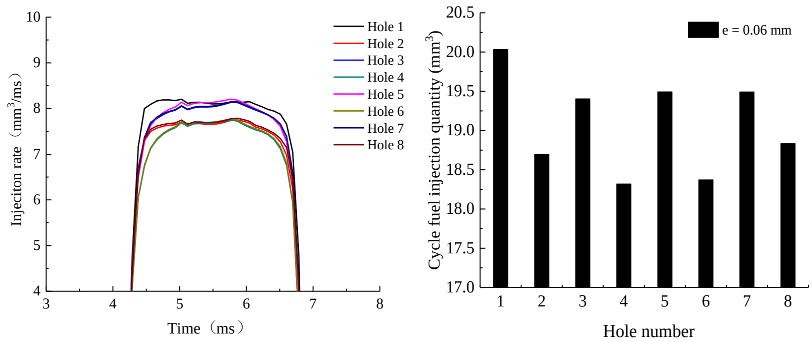

(d) e=0.06mm (45° deflection)

Fig. 15 Injection rate (left) and cycle injection quantity (right) of

each hole with different needle eccentric parameters

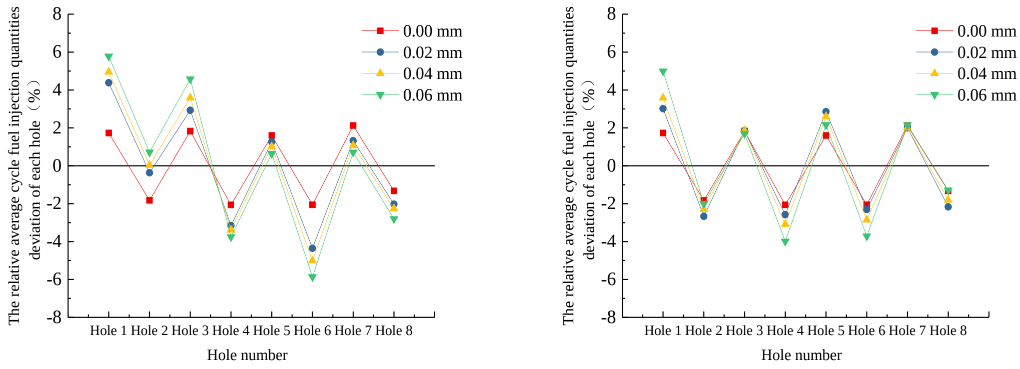

(a) 0° deflection (b) 45° deflection

Fig. 16 The relative average cycle fuel injection quantities deviation of each hole at different eccentric directions

4.3 Effect of needle eccentricity on internal flow characteristics of the nozzle

The development process and distribution of the cavitation within the holes in the same layer are similar with each other as in the Ideal model. When the needle moves eccentrically, the development and distribution of cavitation inside each hole on the upper and lower surfaces of the holes are quite different.

Cavitation is characterized by volume fraction. As the gas volume fraction inside the nozzle hole increases, the cavitation area inside the hole increases. As shown in Tab.3, in Model 1, the cavitation on the upper surface of hole 2 is small, therefore the primary cavitation is on the lower surface of hole 2 at +14 % lift. The fuel from the entrance (upper opening) of the injector sac volume enters the nozzle hole through the bottom while the fuel from the bottom of the injector sac volume enters the nozzle hole through the top. This is as a result of the geometry of the injector sac volume and the nozzle holes. Torelli[42] achieved the same tendency. Low pressure areas (that enables the formation of cavitation) are then created at the top and bottom sections of the nozzle hole (hole 2). Cavitation is hence formed on both sections of hole 2. The degree of cavitation in the upper surface is stronger than the one formed in the bottom surface at 28% lift. At 43% lift, the cavitation at the bottom section of the nozzle hole starts to disappear. Nonetheless, the cavitation in hole 2 is weaker as compared to the cavitation in hole 6. When the needle valve lift is 57 %, the cavitation on the upper surface of hole 2 tend to be stable and the cavitation on the bottom surface almost disappear, leaving only a small part. When the needle valve lift is 71%, the cavitation of hole 2 is stable, which is similar to hole 2 without eccentric movement.

The needle glides along the needle body from +14 %~+28 % lift in Model 2. The extremely narrow flow area in the displaced space causes irregular fuel flow, which results in the formation of cavitation at the bottom surfaces of hole 2. As the needle lifts vertically, the position of the cavitation gradually changes from the lower surface to the upper surface of hole 2 with the gradual increase of the flow area in the displaced space. From +14% to +28% lift, the cavitation formation at the bottom surface is higher. At +43% lift, the cavitation of hole 2 reduces to half the cavitation at +14% lift. At +57 % lift, weak cavitation formations appear on the upper and bottom sections of hole 2. At +71 % lift, the cavitation in nozzle hole 2 almost disappear, leaving tiny cavitation formations on both upper and bottom surfaces.

Tab.3 The cavitation distribution inside holes with different needle motion models（e=0.06mm）

Lift	Ideal model	Model 1	Model 2
+14 %	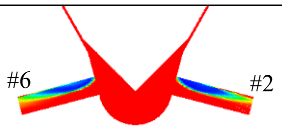	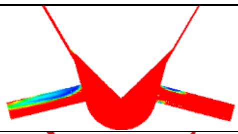	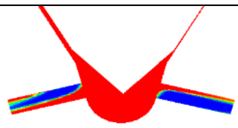
+28 %	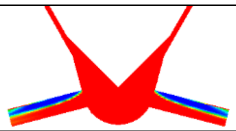	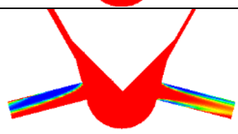	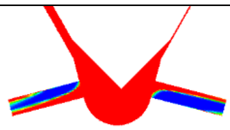
+ 43%	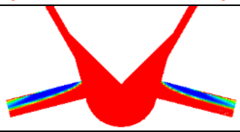	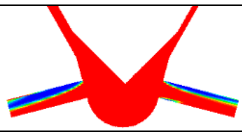	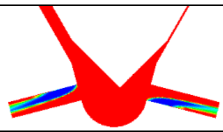

+ 57%	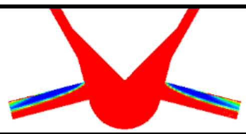	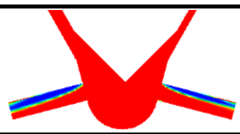	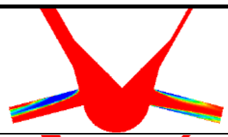
+ 71 %	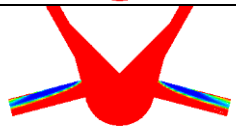		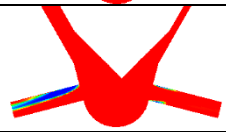
+ 86 %	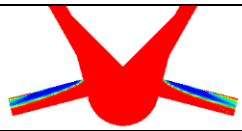	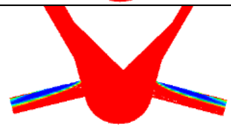	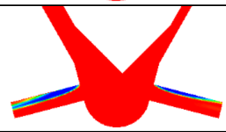
+100 %	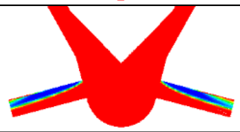		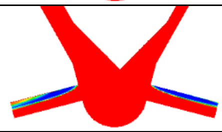

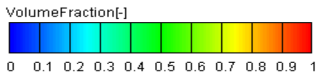

As shown in Tab.4, the fuel flow velocity inside hole 2 is higher than the upper and lower surface of hole 2 in Model 1due to the cavitation formation at the upper and lower surfaces at 28 % needle lift. The flow velocity within each nozzle hole during full needle lift is more uniform as compared to the flow velocities at the initial stages of needle lift in Model 1.

In Model 2, high-velocity region in hole 2 is less at + 28 % due to the irregular flow at the initial stage of the needle lift. The fuel flows into the upper side of hole 2 because of the guiding effect of the sac and the hole structure. The high- velocity region inside the hole 2 gradually transfers from the upper surface to the lower surface with the increment of the displaced flow area due to the changing effect of cavitation at those areas.

Tab. 4 The velocity distribution inside holes with different needle motion models（e=0.06mm）.

Lift	Ideal model	Model 1	Model 2
28 %	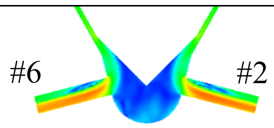	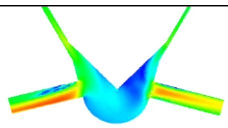	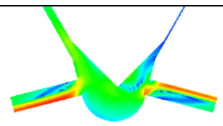
43 %	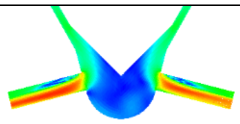	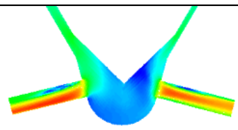	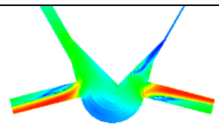

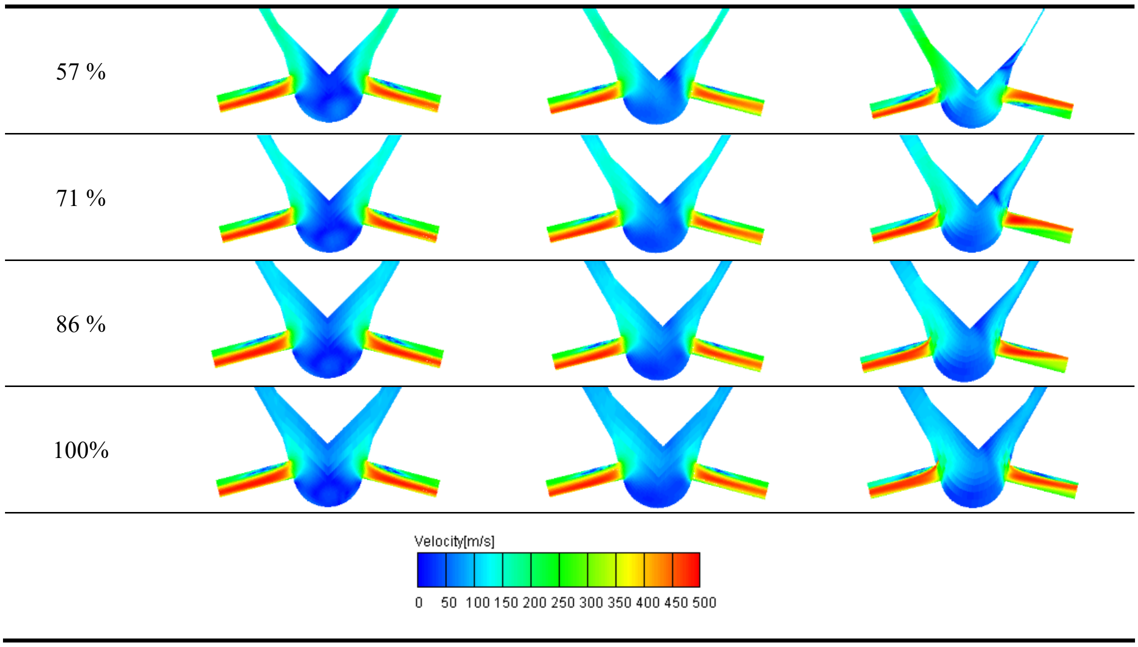

5 Conclusion

A three-dimensional (3-D) model of a nozzle which was validated with experimental results was used to analyze the injection characteristics of each hole. Two different needle eccentricity models based on inelastic deformation of the needle were established to analyze the effect on the fuel injection characteristics and internal flow characteristics of each nozzle hole. The first method only considered the lateral displacement of the needle during needle lift. The needle reached the largest eccentricity at the maximum lift. The second method took the needle inelastic deformation into consideration. That is, the needle radially displaces and glides along with the needle seat surface during needle lift. At maximum radial displacement, the needle lifts vertically upward from the displaced position. From the result the following were observed：

1. Each eccentricity models led to asymmetric fuel flow. The transient injection rate differences between the nozzle holes hole becomes more apparent as the eccentricity increases. In Model 1, the injection rate of hole 2 (The nozzle hole closest to the needle displacement) rises rapidly during the opening process. In Model 2, the injection rate of hole 2 in the initial stages of the needle lift is lower than the injection rates from the other

nozzle holes in the same layer. At full needle lift, the fuel injection rate of hole 2 is higher than those from the other injection holes in the same layer.

2. The cycle fuel injection quantity of hole 2 increases as the eccentricity of the needle increases in Model 1. The cycle fuel injection quantity of hole 6 (the nozzle hole farthest from the needle displacement) decreases as the eccentricity of the needle increases. Resulting in increasing non-uniformity in fuel injection. The upper layer holes are highly affected by the needle eccentricity, comparatively.
3. The cavitation distribution within the nozzle holes in the two needle eccentricity models are quite different. In the first eccentric model, the cavitation intensity of hole 2 is weaker than the one formed in hole 6. The difference gradually disappears when the needle is fully opened. In the second eccentricity model, the cavitation of hole 2 first appears on the lower side at the initial stages and gradually shifts to the upper side as the lifting progresses.

Acknowledgments

This work is supported financially by the National Natural Science Foundation of China (No. 51476072)

References

[1] Tay, K.L., Yang, W., Zhao, F., Yu, W., and Mohan, B., 2017, “Effects of triangular and ramp injection rate-shapes on the performance and emissions of a kerosene-diesel fueled direct injection compression ignition engine: A numerical study,” Appl. Therm. Eng, 110, pp.1401–1410. doi: 10.1016/j.applthermaleng.2016.09.072.

[2] Wang, G., Yu, W., Li, X., and Yang, R., 2020, “Influence of fuel injection and intake port on combustion characteristics of controllable intake swirl diesel engine,” Fuel, 262, p. 116548. doi:

10.1016/j.fuel.2019.116548.

[3] Luo, T., Jiang, S., Moro, A., Wang, C., Zhou, L. and Luo, F., 2018, “Measurement and validation of hole-to-hole fuel injection rate from a diesel injector,” Flow Meas. Instrum, 61, pp.66–78. 10.1016/j.flowmeasinst.2018.03.014.

[4] Huang, W., Moon, S., Gao, Y., Li, Z. and Wang, J., 2017, “Eccentric needle motion effect on near-nozzle dynamics of diesel spray,” Fuel. 206, pp. 409–419. 10.1016/j.fuel.2017.06.012.

[5] Battistoni M., Som S. and Powell C F.,2019, “Highly resolved Eulerian simulations of fuel spray transients in single and multi-hole injectors: Nozzle flow and near-exit dynamics,” Fuel, 251, pp. 709-729. 10.1016/j.fuel.2019.04.076.

[6] Chiatti, G., Chiavola, O., Palazzoni, M. and Palmieri, F ,2015, “Diesel spray modeling under off-axis needle displacement,” SAE Tech. Pap, No.2015-01-0922. 10.4271/2015-01-0922.

[7] Chiavola, O. and Palmieri, F., 2017, “On a Modified VCO Nozzle Layout for Diesel Common Rail Injectors under Actual Needle Displacement,” Energy Procedia, 126, pp. 1027–1034. https://doi.org/10.1016/j.egypro.2017.08.309. 10.1016/j.egypro.2017.08.309.

[8] Salvador, F. J., Martinezlopez, J., Caballer, M. and De Alfonso, C., 2013, “Study of the influence of the needle lift on the internal flow and cavitation phenomenon in diesel injector nozzles by CFD using RANS methods,” Energy Convers. Manag., 66, pp. 246–256. 10.1016/j.enconman.2012.10.011.

[9] Wang, C., Moro, A., Xue, F., Wu, X. and Luo, F., 2018, “The influence of eccentric needle movement on internal flow and injection characteristics of a multi-hole diesel nozzle,” Int. J. Heat Mass Transf., 117, pp.818–834. https://doi.org/10.1016/j.ijheatmasstransfer.2017.10.057.

[10] Moro, A., Luo, T., Wang, C. and Luo, F., 2019, “Eccentric needle displacement effect on spray formation from a multi orifice diesel injector,” Heat Mass Transf, 55(9), pp. 2623-2635. 10.1007/s00231-019-02584-3

[11] Salvador, F.J., Martinezlopez, J., Romero, J.V. and Rosello, M.D., 2014, “Study of the influence of the needle eccentricity on the internal flow in diesel injector nozzles by computational fluid dynamics calculations,” Int. J. Comput. Math., 91(1), pp. 24-31. 10.1080/00207160.2013.770483.

[12] Torelli, R., Som, S., Pei, Y., Zhang, Y. and Traver, M., 2017, “Influence of fuel properties on internal nozzle flow development in a multi-hole diesel injector,” Fuel, 204, pp. 171–184. 10.1016/j.fuel.2017.04.123.

[13] He, Z., Xuan, T., Xue, Y. and Liang Z. 2014, “A numerical study of the effects of injection rate shape on combustion and emission of diesel engines,” Therm. Sci., 18(1), pp. 67-78. 10.2298/TSCI130810013H.

[14] Yao, C., Geng, P., Yin, Z., Hu, J., Chen, D. and Ju, Y., 2016, “Impacts of nozzle geometry on spray combustion of high pressure common rail injectors in a constant volume combustion chamber,” Fuel, 179, pp. 235–245. 10.1016/j.fuel.2016.03.097.

[15] Zhang, X., He, Z., Wang, Q., Tao, X., Zhou, Z., Xia, X. and Zhang, W., 2018, “Effect of fuel temperature on cavitation flow inside vertical multi-hole nozzles and spray characteristics with different nozzle geometries,” Exp. Therm. Fluid Sci., 91, pp. 374–387. 10.1016/j.expthermflusci.2017.06.006.

[16] Xue, F., Luo, F., Cui, H., Moro, A. and Zhou, L., 2017, “Numerical analyses of transient flow characteristics within each nozzle hole of an asymmetric diesel injector,” Int. J. Heat Mass Transf, 104, pp. 18–27. 10.1016/j.ijheatmasstransfer.2016.08.027.

[17] Salvador, F.J., Lopez, J.J., De la Morena, J and Crialesi-Esposito, M., 2018, “Experimental investigation of the effect of orifices inclination angle in multihole diesel injector nozzles. Part 1 – Hydraulic performance,” Fuel. 213, pp. 207–214. 10.1016/j.fuel.2017.04.019.

[18] Payri, R., Salvador, F.J., De la Morena, J.and Pagano, V., 2018, Experimental investigation of the effect of orifices inclination angle in multihole diesel injector nozzles. Part 2 – Spray characteristics,” Fuel. 213, pp. 215–221. 10.1016/j.fuel.2017.07.076.

[19] Pelletingeas, A., Dufresne, L.and Seers, P., 2016, “Characterization of flow structures in a diesel injector for different needle lifts and a fluctuating injection pressure,” J. Fluids Eng. Trans. ASME, 138(8), p. 08115. 10.1115/1.4033125.

[20] Moon, S., Zhang, X., Gao, J., Fezzaa, K., Durfresne, E., Wang, J.and Lai, M. C., 2015, “Morphological exploration of emerging jet flows from multi-hole diesel injectors at different needle lifts,” At. Sprays, 25 (5), pp. 375-396. 10.1615/AtomizSpr.2015011058.

[21] Moon, S., Gao, Y., Park, S. H., Wang, J., Kurimoto, N.and Nishijima, Y., 2015, “Effect of the number and position of nozzle holes on in- and near-nozzle dynamic characteristics of diesel injection,” Fuel, 150, pp. 112–122. 10.1016/j.fuel.2015.01.097.

[22] Kastengren, A.L., Powell, C.F., Liu, Z., Fezzaa, K. and Wang, J., 2009, “High-speed X-ray imaging of diesel injector needle motion,” ASME 2009 Internal Combustion Engine Division Spring Technical Conference, Milwaukee, Wisconsin, USA. May 3–6. pp. 247–258. 10.1115/ICES2009-76032

[23] Huang, W., Moon, S.and Ohsawa, K., 2016, “Near-nozzle dynamics of diesel spray under varied needle lifts and its prediction using analytical model,” Fuel, 180, pp. 292–300. 10.1016/j.fuel.2016.04.042.

[24] Salvador, F.J., De la Morena, J., Crialesi-Esposito, M.and Martínez-López, J., 2018, “Comparative study of the internal flow in diesel injection nozzles at cavitating conditions at different needle lifts with steady and transient simulations approaches,” Proc. Inst. Mech. Eng. Part D J. Automob. Eng., 232, pp. 1060–1078. doi: 10.1177/0954407017725672.

[25] Viera, J. P., Payri, R., Swantek, A. B., Duke, D. J., Sovis, N., Kastengren, A. L. and Powell, C. F., 2016, “Linking instantaneous rate of injection to X-ray needle lift measurements for a direct-acting piezoelectric injector,” Energy Convers. Manag., pp.350–358. 10.1016/j.enconman.2016.01.038.

[26] Arienti, M.and Sussman, M., 2017, “A numerical study of the thermal transient in high-pressure diesel

injection," Int. J. Multiph. Flow, 88, pp.205–221. 10.1016/j.ijmultiphaseflow.2016.09.017

[27] Kastengren, A.L., Tilocco, Z.F., Powell, C.F., Manin, J.and Bazyn, T., 2012, "Engine combustion network (ECN): measurements of nozzle geometry and hydraulic behavior," At. Sprays, 22, pp. 1011–1052. 10.1615/AtomizSpr.2013006309

[28] Ohnishi, H., Yoshida, T., Arifuku, T.and Kadota, T., 1995, "Characteristics of fuel discharge in multihole VCO nozzle,". Transactions of the Japan Society of Mechanical Engineers B, 61, pp.1554–1559.

[29] Zhang, X., Liu, J. and Wang, J, 2016, "Effect of fuel and nozzle geometry on the off-axis oscillation of needle in diesel injectors using high-speed X-ray phase contrast imaging," J. Instrum, 11 (05), p. C05015. 10.1088/1748-0221/11/05/C05015

[30] Battistoni, M., Xue, Q., Som, S., and Pomraning, E., 2014, " Effect of off-axis needle motion on internal nozzle and near exit flow in a multi-hole diesel injector," SAE Int. J. Fuels Lubr., 7(1), pp. 167-182. 10.4271/2014-01-1426.

[31] Powell, C.F., Kastengren, A.L., Liu, Z.and Fezzaa, K., 2009, "The effects of diesel injector needle motion on spray structure". Proc. ASME Intern. Combust. Engine Div. Fall Tech. Conf., 133, pp. 207–217. 10.1115/ICEF2009-14076.

[32] Kim, B.and Park, S., 2019, "Study on in-nozzle flow and spray behavior characteristics under various needle positions and length-to-width ratios of nozzle orifice using a transparent acrylic nozzle,". Int. J. Heat Mass Transf, 143, p.118478. 10.1016/j.ijheatmasstransfer.2019.118478.

[33] Payri, R., Garcia, A., Domenech, V., Durrett, R. P. and Plazas, A.H., 2012, "An experimental study of gasoline effects on injection rate, momentum flux and spray characteristics using a common rail diesel injection system," Fuel, 97, pp. 390–399. 10.1016/j.fuel.2011.11.065.

[34] Payri, F., Payri, R., Salvador, F. J., and Gimeno, J., 2005, "Comparison between different hole to hole

measurement techniques in a diesel injection nozzle," SAE Tech. Pap, No2005-01-2094. 10.4271/2005-01-2094.

[35] Luo, F., Jiang, S., Moro, A., Luo, T., Zhou, L. and Wu, X., 2017, "The development of a data acquisition system for measuring the injection rate of a multihole diesel injector," Sensors Actuators, A Phys., 261, pp. 166-176. 10.1016/j.sna.2017.04.037.

[36] Wu, X., Deng, J., Cui, H., Xue, F., Zhou, L. and Luo, F., 2016, "Numerical simulation of injection rate of each nozzle hole of multi-hole diesel injector," Appl. Therm. Eng., 108, pp. 793–797. 10.1016/j.applthermaleng.2016.07.136.

[37] Zhou, L., Dong, S. F., Cui, H. F., Wu, X., Xue, F. and Luo, F., 2016, "Measurements and analyses on the transient discharge coefficient of each nozzle hole of multi-hole diesel injector," Sensors Actuators, A Phys., 244, pp. 198–205. 10.1016/j.sna.2016.04.017.

[38] Hanjalic, K., Popovac, M., and Hadžiabdic, M., 2004, "A robust near-wall elliptic-relaxation eddy-viscosity turbulence model for CFD," Int. J. Heat Fluid Flow, 25, pp.1047–1051. 10.1016/j.ijheatfluidflow.2004.07.005

[39] Billard, F. and Laurence, D., 2012, "A robust k-ε-v2/k elliptic blending turbulence model applied to near-wall, separated and buoyant flows," Int. J. Heat Fluid Flow, 33(1), pp. 45–58.

[40] Li, D., Liu, S., Wei, Y., Liang, R. and Tang, Y., 2018, "Numerical investigation on transient internal cavitating flow and spray characteristics in a single-hole diesel injector nozzle: A 3D method for cavitation-induced primary break-up", Fuel, 233, pp.778-795. 10.1016/j.ijheatfluidflow.2011.11.003.

[41] Wang, C., Adams, M., Jin, T., Sun, Y., Roell, A., Luo, F. and Gavaises, M., 2021, "An analytical model of diesel injector's needle valve eccentric motion," Int. J. Engine Res, 2021(1):146808742098736. 10.1177/1468087420987367

[42] Torelli, R., Matusik, K., Nelli, K C., Kastengren, L., Fezzaa, Kamel, K., Powell, F. and Som S., 2018,

"Evaluation of Shot-to-Shot In-Nozzle Flow Variations in a Heavy-Duty Diesel Injector Using Real Nozzle Geometry," SAE Int. J. Fuels Lubr., 11(4), No. 2018-01-0303. 10.4271/2018-01-0303.